Experimental Validation of Numerical Models of Collecting Electrodes

Andrzej P. Nowak
Technical University of Bielsko-Biala
Poland
a.nowak@ath.bielsko.pl

1 Summary / Abstract:

The paper presents an experimental validation of two models of the collecting electrodes of an electrostatic precipitator (ESP). The first model combines the finite element method used for calculations of spring deformations with the rigid finite element method used to reflect mass and geometrical features [11]. It is called the hybrid finite element method (model: *HFEM*). As a result, the model with a diagonal mass matrix is obtained. Due to a specific geometry of the electrodes, which are long plates of complicated shapes, the second model uses the strip method (model: *SPL*). The strip method is a semi-analytical method [2], which allows us to formulate the equations of motion with a considerably smaller number of generalized coordinates. Frequencies of free vibrations calculated by means of both methods were compared in [1]. This paper presents a comparison of results calculated with those from experimental measurements. A short characteristic of the equipment used, the results of measurements and some analysis are presented as well.

2 Introduction

The efficiency of electrostatic precipitators influences the environment. The effectiveness of those devices depends on many factors [[13], [4], [5], [9], [12]. One of them is the efficiency of periodic cleaning of the collecting electrodes – the dust is removed by inducing vibrations. These vibrations are caused by an axial impact of a beater on a brushing bar. Rapping energy is propagated over the rapping system and the electrodes. The author deals with such problems for many years and his interest is the subject of numerous works [6], [2], [8] among others.
Geometrical features of the electrodes and the force impact have an essential influence on tangent and normal accelerations at different points of the electrodes, and thus on the effectiveness of the dust removal process.
This paper presents an experimental validation of two models. The models are formulated using new modelling methods of the collecting electrodes which enable us to analyse vibrations of the system.

2.1 *HFEM* model

The first method called the hybrid finite element method combines the rigid finite element method [11] and the finite element method. The *HFEM* model involves considerably large number of degrees of freedom which effects the calculation time. In order to discretise the plate the coordinate system ***xyz*** is assigned to the electrode as shown in Fig.2-2.

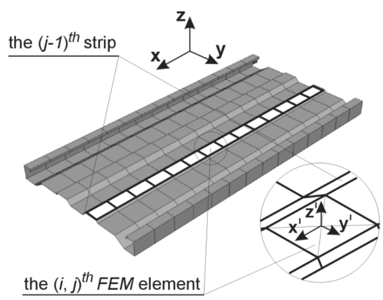

Fig. 2-2: SIGMA electrode

The classical finite element method (*FEM*) is used in order to calculate the energy of spring deformation. To this end, each element (*i*, *j*) is treated as a shell rectangular element (Fig. 2-2), so that the displacements of nodes are described by the following vector:

$$\mathbf{q}^{(s)} = \begin{bmatrix} u_s & v_s & w_s & \varphi_s^x & \varphi_s^y & \varphi_s^z \end{bmatrix}^T \text{ for s=1,2,3,4} \quad (1)$$

where:

- u, v, w are displacements along **x'**, **y'** and **z'** axes respectively,
- **x'y'z'** is a local coordinate system assigned to element (*i*,*j*),
- $\varphi^x, \varphi^y, \varphi^z$ are respective rotations.

The energy of elastic deformation is a sum of energies of elastic strains corresponding to shield $^{(s)}$ and plate $^{(p)}$ states:

$$E = E^{(s)} + E^{(p)} \qquad (2)$$

and after some calculations it can be presented in the form:

$$E = \tfrac{1}{2}\mathbf{q}^T\mathbf{C}\mathbf{q} \qquad (3)$$

where:

$\mathbf{C}$ is a stiffness matrix with 24 x 24 elements,

$\mathbf{q}^{(s)}\big|_{s=1,2,3,4}$ is defined in (1).

In order to reflect mass features of the electrodes the rigid finite element method is used. According to the rigid finite element method the flexible body considered is divided into rigid elements reflecting inertial features of the body and spring-damping elements which connects the rigid elements and adopt spring and damping features.

The equations of motion of the whole system (the electrode plates, brushing bar and the suspension beam), which are formulated using the Lagrange equations, can be written in the form:

$$\mathbf{M}_H\ddot{\mathbf{q}}_H + \mathbf{K}_H\mathbf{q}_H = \mathbf{f}_H \qquad (4)$$

where:

$\mathbf{M}_H$ is the diagonal mass matrix,

$\mathbf{K}_H$ is the stiffness matrix.

The vector of generalized coordinates $\mathbf{q}_H$ has $n_H = 6N$ components, where N *is* the number of rigid finite elements (*rfes*). More details about the *HFEM* can be found in [6].

2.2 *SPL* model

Since geometrical properties do not vary along the length of the electrode the second model is formulated using the strip method, where the deformations in this direction are modelled by means of spline functions. Spline functions B_3 are recommended in [14] as they have some advantages over classical finite element method and semi-analytical strip method, especially: small number of degrees of freedom, continuity of C_2 and easiness of accounting for different boundary conditions. These features lead to numerically effective models. The shape of the electrode, which can be treated as a set of long stripes with different angles of inclination, naturally fits into the method (Fig. 2-3). In order to discretise the plate the coordinate system ***xyz*** is assigned to the electrode as shown in Fig.2-3.

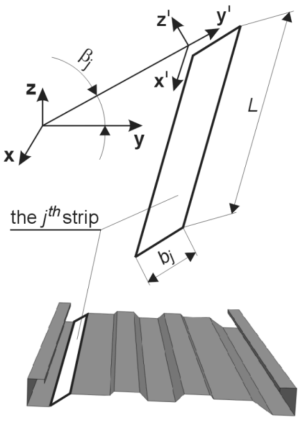

Fig. 2-3: SIGMA electrode

Let us consider the j^{th} strip presented in Fig.2-3 with width b_j, length L and angle of inclination β_j. Deflections in the perpendicular direction to the surface of the strip, i.e. along **z'** axis, are described by the following relation:

$$w_j(x', y') = X_w(x')Y_w^{(j)}(y') \qquad (5)$$

The idea of separation of variables, as in function (5), is often used in vibration analysis of beams, plates and shells for time and spatial variables. Functions are defined using B_3 splines as follows:

$$X_\beta(x') = \sum_{k=-1}^{n+1}\alpha_k\varphi_k(x'), \qquad (6)$$

where:

$\alpha_k = \alpha_k(t)$ are time depended coefficients,

$\varphi_k(x')$ are B_3 splines,

$n=n_x$ is the number of intervals into which the strip is divided (the interval <0, L> is divided into segments with equal length).

After calculating kinetic and spring deformation energies the final equations have to be expressed in the global system and the equations of motion of the electrode are written as:

$$\mathbf{M}_S\ddot{\mathbf{q}}_S + \mathbf{K}_S\mathbf{q}_S = \mathbf{f}_S \qquad (7)$$

where:

$\mathbf{q}_S$ is a vector with $n_S = 4(n+3)m$ elements,

m is the number of strips into which the collecting electrode is divided.

Although matrix $\mathbf{M}_S$ is not diagonal, both $\mathbf{M}_S$ and $\mathbf{K}_S$ are sparse matrices. More details about *SPL* method are presented in [6].

2.3 Test stand

The measurements were performed on a test stand build by a producer of electrostatic precipitators (Fig. 2-4).

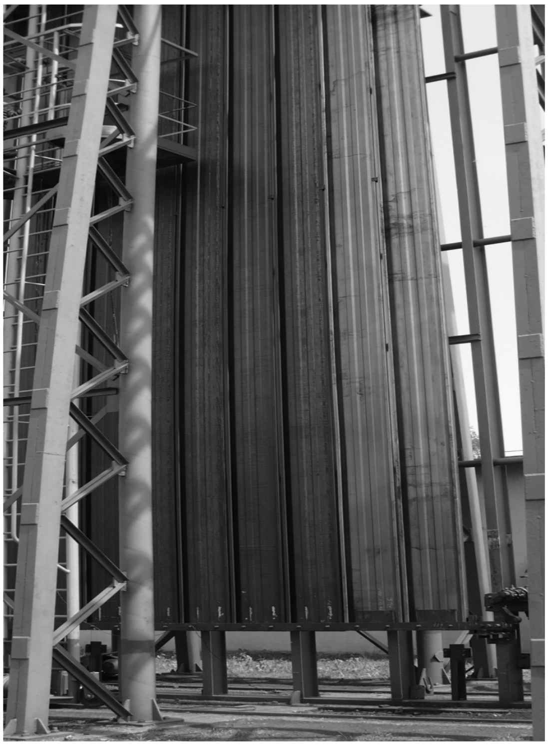

Fig. 2-4: Test stand

The scheme of the measuring system is presented in Fig. 2-5. The system consists of nine collecting electrodes (2) (SIGMA type) suspended on a common beam (1) and buckled at the bottom with a brushing bar (3) tipped with the anvil (4).

2.4 Characteristics of the measuring equipment

The main elements of the measuring system are:

- 16-channel recorder TEAC lx110,
- a portable computer with LX Navi and FlexPro software,
- 5 triaxial vibration ICP sensors (type: 356A02 of PCB Piezotronics).

The signals were recorded with a sampling rate of 24 kHz (per channel), as the answer of the system for a single force impulse $F(t)$ (hammer impact – Fig. 2-5). These events are called series of measurements, or briefly series. The hammer movement was forced manually while the mechanical drive was off. During the measurements signals were recorded for n = 10 to 25 series for each configuration of the sensors (Fig. 2 5 - levels I÷V, perpendiculars $S_{1\text{-}C}$÷$S_{5\text{-}C}$ and $S_{1\text{-}L}$÷$S_{5\text{-}L}$). The CP_{4C}^{L3} stands for a checkpoint on the third level and the fourth-C perpendicular.

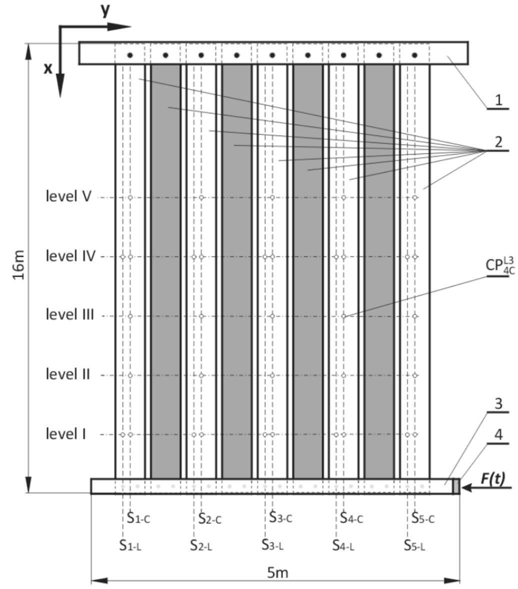

Fig. 2-5: Scheme of the measuring system

2.5 Experimental measurements

Since it was impossible to activate recording of signals automatically, the courses obtained had to be synchronized. Fig. 2.6 shows 10 courses of component a_z registered by sensor $S_{1\text{-}C}$ on electrode 1 (before and after synchronization).

a)

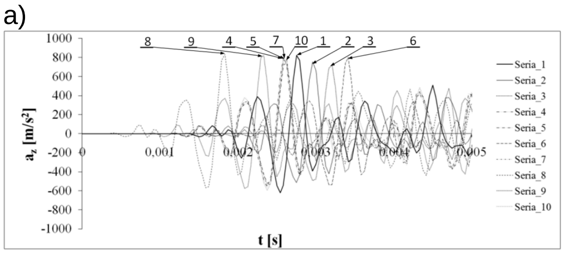

b)

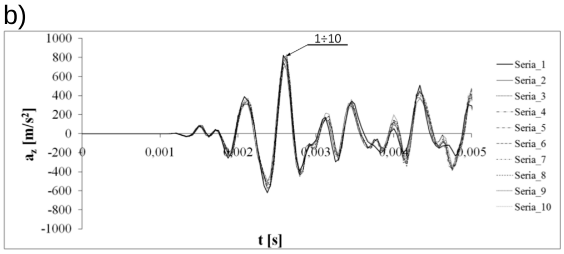

Fig. 2-6: Courses of a_z:

a) before synchronization
b) after synchronization

For both the producers and contractors, the primary criterion for the evaluation of the effectiveness of surface cleaning are the maximal values of the acceleration normal to the surface of the electrode. It is generally accepted that the rapping system works well, if at any point of the control section, the maximum value of normal acceleration is greater than 100*g* (*g* - acceleration due to gravity). This approach was often forced by the low class of applied measuring equipment. Nowadays, because of the development of the measurement technology, the values of the other components of acceleration are taken into account more and more often. In this paper pre-processed signals are used to determine the maximum value of all the acceleration components as well as the total acceleration at the checkpoints for *n* series. These results are used for validation of the numerical models of the collecting electrodes. Especially amplitudes and periods of acceleration are evaluated. The details of the methodology are presented in [7].

3 Validation of the models

Results of numerical calculations obtained by means of both models (*HFEM* and *SPL*) were compared with those from the measurements (*VAL*). Force impulse *F*(*t*) was measured and assumed to be as shown in Fig. 3-1.

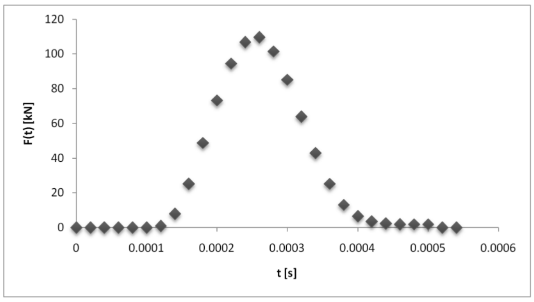

Fig. 3-1: Force impulse *F*(*t*)

The comparison is made using *runRMS* and *RMS* (root-mean-squared) values as well as factor *k* (FAC_k) and the hit rate q_ε.

3.1 runRMS criterion

Fig. 3-2 shows time courses of *runRMS* for the signals, which were obtained from simulations (*HFEM* and *SPL*) and measurements (*VAL*). *RunRMS* time courses were calculated for the total accelerations at the selected checkpoints. These type of time courses allow us to determine the maximum values of *runRMS* (marked as: $runRMS_{MAX}$).

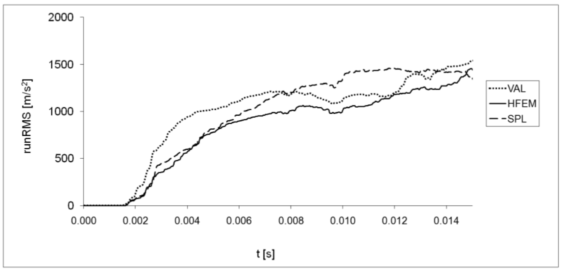

Fig. 3-2: *RunRMS* courses

In further analysis $runRMS_{MAX}$ values are compared (Fig. 3-3). These values were calculated at 5 checkpoints for total accelerations.

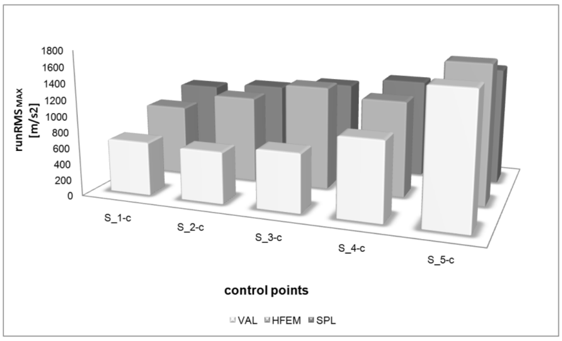

Fig. 3-3: $RunRMS_{MAX}$ values

3.2 FAC_k and q_ε

Pre-processed measured signals are used for validation of the numerical models. However, basing on the analyses carried out, it is impossible to obtain an agreement between the results of numerical simulation and the measurements. A direct comparison of time courses of accelerations has to be replaced with other measure. For this reason, the quantitative analysis of the results is carried out by means of two different indicators.

FAC_k is defined as follows [3]:

$$FAC_k = \frac{1}{n}\sum_{i=1}^{n}\begin{cases} 1 & for\ \ \frac{1}{k} \le \frac{RMS|_{i^{(s)}}}{RMS|_{i^{(m)}}} \le k \\ 0 & otherwise \end{cases} \tag{8}$$

where:

$RMS|_{i^{(s)}}$ - *RMS* value calculated for the i^{th} simulation signal

$RMS|_{i^{(m)}}$ - *RMS* value calculated for the i^{th} measurement signal

k - boundary coefficient (k = 1÷3)

n - number of points.

Hit rate q_ε is a second indicator which is also used for model validation. It is used, among others, to evaluate the forecasting micro-scale models [10] and it is defined in the form:

$$q_\varepsilon = \frac{1}{n}\sum_{i=1}^{n}\begin{cases}1 & \text{for} \quad \left|\dfrac{RMS\big|_{i^{(s)}} - RMS\big|_{i^{(m)}}}{RMS\big|_{i^{(m)}}}\right| \le \varepsilon \\ 0 & \text{otherwise}\end{cases} \quad (9)$$

where ε is a maximum relative error assumed (ε=*0.1÷0.5*).

3.3 Validation results

The results of the model validation presented below were obtained assuming the following values of validation parameters:

k = 2,

n = 35 (all measuring points),

$\varepsilon = 0.4$.

Fig. 3-4 presents the values of FAC_k indicator for normal and total accelerations.

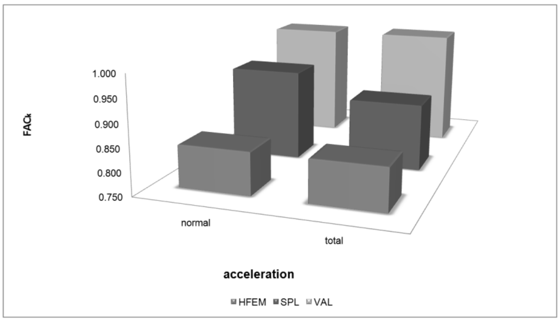

Fig. 3-4: FAC_k indicator

It can be seen that for the parameters assumed, *SPL* model is more accurate than *HFEM* model with respect to FAC_k criterion Approximately 95% of the checkpoints in the case of normal accelerations, and about 90% of the checkpoints in the case of total accelerations fall within the accepted range of values. In the case of *HFEM* model these values are lower by about 10% and 5% respectively.

Hit rate q_ε indicator highlights the differences in the accuracy of these models much stronger then FAC_k (Fig. 3-5).

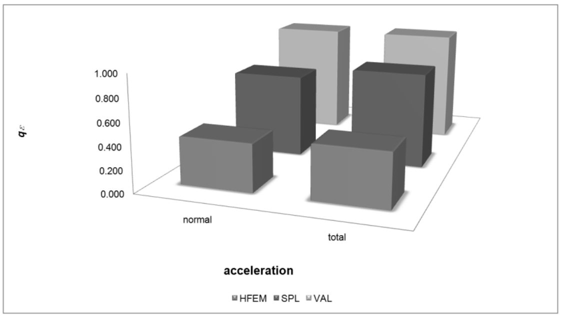

Fig. 3-5: q_ε indicator

For *SPL* model, according to this criterion, approximately 74% of the checkpoints (in the case of normal accelerations) and about 84% of the checkpoints (in the case of the total accelerations) fall within the accepted range of values. For *HFEM* model these values are much lower and they are about 42% and 47% respectively.

4 Final remarks

The paper presents an experimental validation of two numerical models of the collecting electrodes of ESP, which allow us to calculate vibrations of collecting electrodes. The main ideas of the methods have been briefly described. In the hybrid finite element method proposed the finite element method is used for calculations of spring features while the inertial features are modelled using the rigid finite element method. As a result the model with a diagonal mass matrix is obtained. The strip method allows us to formulate the equations of motion with a considerably smaller number of generalized coordinates. The pre-processed measured signals were used to determine the maximum values of the components and total accelerations at the checkpoints. Comparison of time courses (*runRMS*) and indicator values (FAC_k, q_ε) obtained by means of own methods (*HFEM*, *SPL*) and measurements proves the correctness of both models. In the author's opinion the strip method may be very efficient in the analysis of forced vibrations of the collecting electrodes.

Both methods, despite differences in accuracy, can be used for preliminary evaluation of constructions (new or modified). They allow us to simulate (in a relatively short time) the behaviour of the electrode system under the influence of an applied force impulse.

Accuracy of results obtained by means of both models is comparable to that from commercial packages (ABAQUS, ANSYS), while computation cost is much lower.

5 Literature

[1] Adamiec–Wójcik I., Nowak A., Wojciech S.; Comparison of methods for vibration analysis of electrostatic precipitators; Acta Mechanica Sinica, Issue 1, Springer; 2011; pp. 72-79

[2] Adamiec–Wójcik I., Nowak A., Wojciech S.; Dynamic analysis of electrostatic precipitators using finite strip method; DSTA 2009 Conference Proceedings, Vol. 2; Łódź, Poland; 2009; pp. 889–896

[3] Britter R., Schatzmann M. (ed); Background and justification document to support the model evaluation guidance and protocol; COST Action 732, COST Office, Brussels; 2007

[4] Long, Z., Yao, Q., Song, Q., Li, S.; A second-order accurate finite volume method for the computation of electrical conditions inside a wire-plate electrostatic precipitator on unstructured meshes; Journal of Electrostatics 67(4); 2009; pp. 597-604

[5] Neimarlija, N., Demirdžić, I., Muzaferij, S.; Finite volume method for calculation of electrostatic fields in electrostatic precipitators; Journal of Electrostatics 67(1); 2009; pp. 37-47
[6] Nowak A.P., Adamiec–Wójcik I.; Vibration analysis of collecting electrodes of precipitators by means of the hybrid finite element method; Multibody Dynamics, ECCOMAS Thematic Conference; Warsaw, Poland; 2009; pp. 214-217
[7] Nowak A.; Measuring evaluation of vibration quality of the collecting electrodes section in ESP (in Polish); Measurement Automation and Monitoring; Warszawa; 2011; in print
[8] Nowak A.P., Wojciech S.; Optimisation and experimental verification of a dust-removal beater for the electrodes of electrostatic precipitators; Computers and Structures, Volume 82, Issue 22; 2004; pp. 1785-1792
[9] Talaie, M.R.; Mathematical modelling of wire-duct single-stage electrostatic precipitators; Journal of Hazardous Materials 124 (1-3); 2005; pp. 44-52
[10] VDI Guideline on environmental meteorology – Prognostic microscale wind fields – Evaluation for flow around buildings and obstacles; 3783 Part 9; Düsseldorf; 2005
[11] Wittbrodt, E., Adamiec-Wójcik, I., Wojciech, S.; Dynamics of flexible multibody systems Rigid finite element method. Springer, Berlin Heidelberg New York (2006)
[12] Yang, XF., Kang, YM., Zhong, K.; Effects of geometric parameters and electric indexes on the performance of laboratory-scale electrostatic precipitators; Journal of Hazardous Materials 169 (1-3); 2009; pp. 941-947
[13] Zhao X., Luo S.; A Discussion on the ESP-FF Hybrid Precipitator; Electrostatic Precipitation Precipitator, 11th International Conference on Electrostatic Precipitation (ICESP XI); Zhejiang University Press - Springer, Hagzhou, China; 2008; pp. 472-474
[14] Zienkiewicz, O.C., Taylor, R.L.;The finite element method; Vol.2, Solid Mechanics; Bulterworh-Heinemann; 2003